Surface characterization in Additive Manufacturing

An emperical study of angular dependency

Petter Karlow Herzog

DIVISION OF PRODUCT DEVELOPMENT | DEPARTMENT OF DESIGN SCIENCES
FACULTY OF ENGINEERING LTH | LUND UNIVERSITY
2018

MASTER THESIS

Surface characterization in Additive Manufacturing

An empirical study of angular dependency

Petter Karlow Herzog

November 26, 2018

LUNDS
UNIVERSITET

Surface characterization in Additive Manufacturing
An empirical study of angular dependency.

Published by
Department of Design Sciences
Faculty of Engineering LTH, Lund University
P.O. Box 118, SE-221 00 Lund, Sweden

Publicerad av
Institutionen för designvetenskaper
Lunds Tekniska Högskola, Lunds universitet
Box 118, 221 00 Lund

Subject : Product Development (MMKM05)
Division: Product Development
Supervisor: Olaf Diegel
Examiner: Axel Nordin

Ämne: produktutveckling (MMKM05)
Avdelning: produktutveckling
Handledare: Olaf Diegel
Examinator: Axel Nordin

Abstract

Surface roughness is one of the main challenges for the growing industry of additive manufacturing. Not only are surfaces rougher than on components produced by conventional means, there is also a great variation within a single component as well. In this thesis we have studied the surface roughness of AM components using focused variant microscope and X-ray computer tomography. This is used to find a suitable test component and a measurement protocol to accurately understand and predict the surface roughness produced under specific conditions. The main focus have been on how surface roughness of the external surfaces varies with the angle of the surface. It has been shown that the roughness do depend on the angle of the measured surface and that it is possible to simulate this using simple models, and the measurements necessary could be done in an afternoon. XCT gave an indication that it might be possible to determine the internal surface by measuring the external, however, this we where unable to confirm. From these results the need for an new notation for the roughness parameters became evident and hence we have found a suitable notation which is presented here. The new notation will hopefully make it easier to discuss and communicate which roughness and surfaces that are alluded. This new protocol will give a fast method for understanding and predicting the surface roughness of a new machine or a new set of settings.

Sammanfattning

Ytsträvhet är en utav de absolut största utmaningarna för den växande industrin Friformsframställning (FF). Inte enbart är ytorna utav komponenter framställda med friformsframställning strävare än de framställda med konventionella metoder, det finns dessutom en stor variation inom en komponent. I denna undersökning har vi studerat ytsträvheten hos komponenter framställda genom FF. Detta genom att använda focused variant microsocpe (FVM) och röntgen datortomografi. Målet är att ta fram en testkomponent som kan användas för att förstå och förutsäga ytsträvhet under bestämda förhållanden där huvudfokuset ligger på externa ytor och ytsträvhetens vinkelberoende. Vi har visat att ytsträvheten är vinkelberoende, att detta enkelt kan modelleras och att de nödvändiga mätningarna kan göras på en eftermiddag. Röntgentomografin indikerade att det kan vara möjligt att bestämma ytsträvheten på interna ytor genom att mäta externa, detta kunde vi dock ej bekräfta. Utifrån dessa resultat kunde vi se att behovet av en ny notation var stort, vilken också presenteras här. Den nya notationen kommer förhoppningvis göra det lättare att diskutera och förstå vilken strävhetsparameter och vilken yta som åsyftas. Det protokoll som presenteras här kommer förhoppningsvis göra det möjligt att snabbt och enkelt förstå och förutse ytsträvheten hos en ny maskin eller nya inställningar.

Acknowledgments

I would like to express my deep gratitude to Professor Olaf Diegel for initiating the project, finding an area with in Additive Manufacturing which utilized my previous studies and my interests, and for supporting and guiding me throughout the project.

I would also like to thank the department of industrial production for letting me use their FVM microscope and a special thanks to Henrik Persson for taking me under his wings and teaching me how to use the equipment. An additional thanks to Professor Stephen Hall for the help with doing the XCT measurements and for his help with both analyzing this data but also giving his input on how to improve the test object.

Finally, I wish to thank my family and friends for supporting me throughout my studies.

Contents

1 List of acronyms and abbreviations

AM additive manufacturing. 4

CAD computer aided design. 4

CAM computer aided manufacturing. 4

CCD charge couple device. 10

CNC computer numerical control. 4

FEM finite element method. 6

FVM focused variant microscope. 5

PBF powder bed fusion. 4

R$_a$ arithmetical mean height. 7

R$_p$ maximum Peak height. 7

R$_q$ root mean square height. 7

R$_v$ maximum pit height. 7

RMS root mean square. 10

S$_a$ arithmetical mean height. 8

S$_p$ maximum peak height. 8

S$_q$ root mean square height. 8

S$_v$ maximum pit height. 8

S$_z$ maximum height. 8

S$_{10z}$ ten point height. 8

S$_{dq}$ root mean square gradient. 8

S$_{dr}$ developed inter-facial area ratio. 8

S$_{ku}$ kurtois. 8

S$_{sk}$ skewness. 8

SLM selective laser melting. 4

SLS selective laser sintering. 4

XCT X-ray computed tomography. 5, 14

2 Introduction

Free form manufacturing or in layman's terms 3D printing is thought to be part of the fourth industrial revolution.[7] The first example of some kind of free form manufacturing comes from the late 20th century, during which techniques using contour maps was developed.[1] Layering sheets of wax to form a 3D mould, which could then be used to create topographic maps. Today these ideas have been refined and digitized and are summarized under the name additive manufacturing (AM). This is today primarily done with plastic material, however, can be done with both ceramic, composites and metal materials.[5; 10; 29; 30]

The foundation of the techniques used today was developed in the 1980s, these techniques were mainly used for rapid prototyping by engineers and designers. By the early 2000s, a normal desktop computer could do the calculations needed for a simple 3D design.[17] The technical development reduce cost and soon the 3D printer became a household appliance.[1] However, AM or 3D printing is still mainly used with plastic materials and for prototyping.[17] For industrialization, AM using metal have risen as a contender. We are thought to be at the brink of this revolution, however, there are still a few challenges and more work is needed before AM can become a true contender in serial production.[2]

The aerospace industry, prosthetics industry, and the automotive industry have seen great promise and shown interest in metal AM.[7; 26] In combination with the use of computer aided design (CAD) and computer aided manufacturing (CAM), AM production of complex components can be very useful, highly efficient and possible environmental friendly.[2] The advantage of this technique is the possibility to produce for instance individual implants to match a persons anatomy, or components which have many parts can be reduced to very few. One example is a single piece heat exchanger or anatomical dental implants[20; 24].

AM of metal can be done using several different methods which either produces finished components or green bodies. [7] The green bodies are formed using a binder or pressure and they then have be sintered to form fully dense components. When producing finished components melting is done by using an energy source such as an electron beam or more commonly a laser beam. The material can be applied either directly into the nozzle or by adding layers of material. The later is called powder bed fusion (PBF) if powder is the material substrate used.[17] PBF can be done using either an electron energy source or a laser energy then denoted selective laser melting (SLM) or selective laser sintering (SLS).[17] This is the process which this thesis will focus on and the acronym SLM will be used.

2.1 Scope of the Thesis

SLM is the techniques that produce the best results both in terms of toughness and density. It has been shown that it is possible to achieve similar or better, tensile strength, and yield strength in AM production, when compared to more conventional methods.[10] Several different metals can be used in SLM, however, titanium alloys, aluminum alloys and steels are the most heavily researched.[10] There is one area which is a major drawback of AM and that is the surface roughness, especially when comparing AM to subtractive methods such as computer numerical control (CNC) machining.[14]

Surface roughness is one key feature in the production and the use of a product, since rough-

ness increase wear, friction and the risk for corrosion.[17] In the most promising fields for applying SLM production, medical implants, mechanical components and designs with complex internal geometries, understanding roughness is key.[10] In medical applications sterilization is needed, and to be able to sterilize a metal component a very low surface roughness is necessary.[4] Surface roughness does also decrease the fatigue resilience of mechanical components such as gears and can also lead to an increased risk of corrosion.[22; 28] Eliminating or decreasing the surface roughness is therefore of interest and one step in achieving this is to be able to predict surface roughness. Roughness of the surfaces are believed to be dependent on the direction of the printed surface.

In this thesis we attempt to design a simple test object which allows the user to determine and predict the roughness of the particular process, machine or material used. To be able to measure the roughness a measurement protocol needs to be established. This should be applicable on internal, external, downwards facing, and upwards facing surfaces. In order to make this work accessible and understandable, a simple mathematical model of the measured parameters is needed to give a intuitive overview of what surface roughness to expect at each angle.

We want to provide a useful tool for designers so that they can control and optimize the surface roughness prior to manufacturing components or products. Using focused variant microscope (FVM) to determine extended surface roughness parameters and X-ray computed tomography (XCT) to understand how surface roughness on external surface transfers to internal surfaces. By studying this we also hope to find a way to more accurately describe and discuss surface roughness and derive a suitable notation if needed.

3 Background

3.1 Previous work - Surface roughness

When discussing surface roughness and additive manufacturing the surfaces are usually divided into two different categories. Based on whether they are facing towards the coater and laser source or if they are facing away from the coater and laser source. The surfaces which faces the coater are commonly known as upskin surfaces and the surfaces which faces away are known as downskin surfaces. [3]

Attempts have been made trying to model and predict the surface roughness, using both the melt pool dynamics, modeling the so-called stair-step effect and empirical models.[3; 12; 21; 27] A staircase can be used to describe the surfaces produced in the SLM process, where each layer is a step. In a surface with a steep slope the steps will be shorter and in a less steep surface the steps will be longer. This is called the stair step effect and can be used to understand surfaces in SLM.[27] Different materials have been used in these models. Cabanettes et al. [3] and Vandenbroucke and Kruth [27] studied titanium alloys . Strano, Hao, Everson, and Evans [21] and Khairallah, Anderson, Rubenchik, and King [12] studied stainless steel, however, they have all studied SLM.

Strano et al. [21] suggested that the surface roughness, measured with a contact profilometer, is more or less constant on all surfaces with an up-skin slope. They also believed a model

for predicting this behavior can be achieved by combining theoretical and empirical tools. However, Cabanettes et al. [3] has shown that there is a directional dependency to the surface roughness, i.e that the roughness varies with the direction.

An attempt have been done to model the surface roughness in melt extrusion AM, a technique more similar to the filament driven plastic 3D printers than SLM. Turner and Gold [25] attempted this by estimating the stair step effect and the contribution of each layer to the surface profile. This model showed proficient for angles between 30 and 150 degrees and gives the possibility to estimate the roughness based on several parameters.[25] However, melt extrusion AM have a completely different thermodynamic process compared to SLM. Furthermore, the roughness parameters used in this model was the line parameters and in this thesis, the main focus is the extended parameters.

Pagani, Qi, Jiang, and Scott [18], have attempted to redefine the surface roughness parameters for free formed surfaces. They argue that a new definition is necessary to describe these complex surfaces to avoid the need to compensate for irregularities in the surfaces, irregularities such as warped or rounded shapes. They attempted this using a triangulated mesh similar to the mesh technology used in describing the 3D model prior to manufacturing.[18] This could be very important when investigating roughness in very complex components, however, with rather large and flat surfaces the conventional technique works well.

3.2 Selective Laser Melting

SLM is part of the PBF-family and in this technology, metal powder is applied in a single layer. A energy source then moves in the desired pattern to melt and fuse the powder particles. The melting process causes the current layer to be fused into the adjacent layers as well. When the laser moves forward a pool and track of molten material forms. The track is commonly referred to as the weld track and the pool of molten material is referred to as the melt pool. This process is then repeated for as many layers as necessary to form the product. This is the general process for the PBF process and in SLM the energy source is a laser. [10]

In the weld track material continues to flow as the melt pool cools. The surface tension of the melt pool varies with temperature and in the still molten track this gradient forces the material to move which in turn causes an irregular solidification of the material. This effect is called the Marangoni effect and attempts have been made to model this using the finite element method (FEM) and vector analysis.[12] The motion of material can also cause adjacent solid particles to be attracted to the melted material and fuse. This gives rise to the presence of partly melted particles in the weld track, which contributes to the roughness. [12]

The SLM process have been shown to improve the performance of metals.[10] Herzog, Seyda, Wycisk, and Emmelmann [10] showed that most metals, aluminum alloys, titanium alloys and stainless steel, have a higher tensile strength and yield strength than their wrought counterpart. The complex thermodynamics of the process or the intricate microstructure formed can be the reason for this improvement in performance, however, this has not been confirmed. All of these benefits have made AM a highly desirable technique for high-end applications, especially in aviation and aerospace.[26]

Furthermore the lifetime of products produced by AM have been studied.Wycisk, Solbach,

Siddique, Herzog, Walther, and Emmelmann [31] found that the main contribution to fatigue failure of the components is porosities within the components. However, they also found that a significant contribution to the fatigue is the surface roughness. The resilience to failure from fatigue is deemed to be rather good, however, if the roughness can be reduced this could be further improved.[22] Koike et al. [14] noted that whether the energy source was electron or laser affected the fatigue lifetime. However, the roughness was greater for the one produced with electrons which might have contributed to the decrease lifetime.

Lastly the environmental impact of AM has been shown to be lower than that made in production by conventional means.[7] SLM has a low energy consumption since the small laser is rather energy efficient. By only adding the material needed material usage is low. This shows great promise in being a production method in a sustainable future. Furthermore, the possibility to design and optimize production in AM gives the ability to used material much more efficiently which in turn also decreases the environmental impact.[7]

3.3 Test object

Previous attempts have been done to make test objects which can be used to display the performance and limitations of an AM machine or process. However, this work has been primarily done to understand and tune a machine in an attempt to make sure that the geometries are correct.[16] Although surface roughness is generally part of this type of test objects, this is not the main application. In terms of testing the surface roughness Cabanettes et al. [3], Strano et al. [21], Vandenbroucke and Kruth [27], and Khairallah et al. [12] all have suggested different test objects with different benefits.

Internal geometries are thought to be one of the main applications of AM, since complex components could be produced in one single part.[24] This reduces the production cost, number of parts and in the case of channels, reduces the need for gaskets and risk of leaks. Since these internal surfaces are impossible to measure using conventional methods such as FVM or contact profilometer a non-invasive methods such as XCT has been showing promise.[23]

Thompson et al. [23] have suggested a test object to test how roughness can be measured in XCT. However, this object lacks any angular dependency. Consisting of a hollow object which could be disassembled to measure the internal surfaces using conventional methods.[23] Furthermore, if the roughness of externals surfaces can be related to the internal either directly or using some kind of scaling factor it would be possible to use fast and simple methods to determine the roughness of internal surfaces by measuring external.

XCT is a relatively slow technique since it examines the whole material and the time depends on the amount of material. However, it gives information regarding the internal structure of the sample which gives information regarding porosities and weld solidification, which can be very useful to determine the lifetime of a component.[9; 22]

4 Method

4.1 Roughness parameters

The first way to measure surface roughness was to drag a stylus (needle) over the surface to give a line profile. This technique is fast and simple and is called surface profilometer.[15] Using the line profile the roughness along the line can be determined. For its simplicity, this has been the most common type of surface roughness measurements. From the measured line profiles parameters arithmetical mean height (R_a), root mean square height (R_q), maximum pit height (R_v) and,maximum Peak height (R_p) can be calculated.[8]

However, there are some downsides to the line parameters. They only describe the surface along that particular line and they are invasive and the type of stylus has a great effect on the measurements. A rounded stylus would give a rounder profile and there is a substantial risk of damaging both the surface and the stylus when performing the measurements.[8; 15] Today most modern techniques utilize light or laser to achieve these measurements since this is less invasive and more reproducible.[11]

The line parameters can be extended to an areal value, however, to map an entire surface using a contact profilometer is hard and tedious. With modern optical techniques, this is simple and fast.

Extended parameters are denoted with S instead of R. The ones which are investigated in this thesis are arithmetical mean height (S_a), root mean square height (S_q), maximum peak height (S_p), maximum pit height (S_v), maximum height (S_z), ten point height (S_{10z}), skewness (S_{sk}), kurtois (S_{ku}), root mean square gradient (S_{dq}), and developed inter-facial area ratio (S_{dr}). The definitions of these extended parameters are shown in the following equations, where $Z(x, y)$ is the surface profile and A the area of the measured surface.

$$Sa = \frac{1}{A} \int \int_A |Z(x, y)| dxdy \tag{1}$$

$$Sq = \sqrt{\frac{1}{A} \int \int_A Z^2(x, y) dxdy} \tag{2}$$

$$Sp = max(Z(x, y) \tag{3}$$

$$Sv = |min(Z(x, y)| \tag{4}$$

$$Sz = Sp + Sv \tag{5}$$

$$S10z = \frac{\sum_{i=1}^{5}(Sp_i) + \sum_{i=1}^{5}(Sv_i)}{5} \tag{6}$$

$$Ssk = \frac{1}{Sq^3}\left(\frac{1}{A}\int\int_A Z^3(x,y)dxdy\right) \tag{7}$$

$$Sku = \frac{1}{Sq^4}\left[\frac{1}{A}\int\int_A Z(x,y)^4 dxdy\right] \tag{8}$$

$$Sdq = \sqrt{\frac{1}{A}\int\int_A \left[\left(\frac{\partial Z(x,y)}{\partial x}\right)^2 + \left(\frac{\partial Z(x,y)}{\partial y}\right)^2\right]dxdy} \tag{9}$$

$$Sdr = \frac{1}{A}\left(\int\int_A \left(\sqrt{1+\left(\frac{\partial Z(x,y)}{\partial x}\right)^2 + \left(\frac{\partial Z(x,y)}{\partial y}\right)^2} - 1\right)dxdy\right) \tag{10}$$

From these parameters, it is possible to understand the appearance and functionality of a surface. S_a is the average height from the mean plane, generally, the parameter which is usually used to show roughness.[15] It is rather insensitive to large differences whereas S_q is similar measurement however more sensitive to larger differences. S_p shows how high the highest peak is above the mean, S_v the lowest pit below the mean, and S_z the longest distance between the lowest pit and highest peak. S_{10z} shows the average of the five highest peak and five lowest pits. [15]

These parameters are the most used and give a general overview of the surface on their own ,however, they can be combined to understand more about the surfaces. They tell us something regarding whether there are many high peaks if the S_p is similar to S_a, or few high peaks if there is a large difference between S_p and S_a. The same can be seen in the relation between S_a and S_v. A much lower S_{10z} than S_z indicates that there are very few high peaks.

The S_{sk} describes the skewness or the degree of bias of the roughness shape i.e. if the peak or pits are symmetrical around the mean plane or have a bias towards one side. S_{sk} of less than zero describes a bias above the mean plane and larger than zero indicates a bias below the mean plane. In a similar manner, the S_{ku} describes the shape of the peaks and pits, whether they are sharp or round. A value of three describes a normal distribution of sharpness and lower than three gives a rounder surface while a value larger than three a sharper surface.[15]

Finally, the S_{dq} describes the change in S_q or the slope of the surface. A flat or smooth surface has a value of zero and any slope increases this value. S_{dr} describes the increase in surface area, how much larger surface the roughness introduces as compared to a completely flat surface. [15]

4.2 Focused Variant Microscope

The focused variant microscope utilizes a very thin field of focus and for each focus plane an image is captured. The light which is reflected of a surface and is in focus is reflected in one direction whereas light reflected upon a surface which is not in focus will be reflected equally in all directions.[11] By moving the objective in the z-plane each part of the surface that is in focus can be related to a height. By addition of all height and positions a surface is generated.

[11] To achieve a larger and more representative image, several images or surfaces can be stitched together to form what is called an image field.

This crude surface can then be filtered using different Gaussian filters to remove unwanted artifacts such as waviness.[11] With this 3D representation of the surface roughness parameters can be calculated, both the line parameters as well as the extended areal parameters.

4.3 X-ray Tomography

X-rays are generated and collimated to form a divergent x-ray source. The x-rays are then allowed to pass through the sample and a charge couple device (CCD) camera records the intensities. By rotating the sample 360 degrees and recording the intensities it is possible to render a 3D model of the sample. [13]From this 3D model of intensities, it is possible to extract the parts contributing to the surface and estimate or calculate the roughness using these.[23]

XCT is not limited to the unperturbed surface of the sample as the FVM is. It is possible to extract information about the internal structure of the sample as well. This can give information regarding density or completion of the welds. This is done by extracting the portions of interest and using image interpretation techniques to estimate abundance of porosities, or the micro structure in general. In general, the intensity is proportional to density so a crack or a pore would appear brighter/darker than the surrounding solid material.[9] The size of the point source determines the resolution and this is commonly called the voxel size and is the extension of a pixel to three dimensions.[19]

4.4 Root-mean-square fitting

The root mean square (RMS) method was used to fit a function to the different roughness parameters. This method utilizes an iterative algorithm which minimizes the distance of the measured value to a function and then estimates the coefficients of said function. Using these parameters a function can be generated which can estimate the roughness at any angle.[6] If the data is estimated to fit the function in equation 11

$$f(x) = a_0 + a_1 x + a_2 x^2 + a_3 x^3 \tag{11}$$

the general error can be expressed as the expression in equation 12

$$err = \sum (d_j)^2 = (y_1 - f(x_1))^2 + (y_2 - f(x_2))^2 + (y_3 - f(x_3))^2 + (y_4 - f(x_4))^2 \tag{12}$$

we can then rearrange 11 and 12 to express the error as equation 13

$$err = \sum_{i=1}^{h} \left(y_i - \left(a_0 + a_1 x_i + a_2 x_i^2 + a_3 x_i^3 + ... + a_j x_i^j \right) \right)^2 \tag{13}$$

This can then be further simplified to equation 14

$$err = \sum_{i=1}^{n} \left(y_i - \left(a_0 + \sum_{k=1}^{j} a_k x^k \right) \right)^2 \tag{14}$$

From equation 14 it is possible to determine the coefficients a_0, a_1, a_2, a_3.

5 Design

As previously described, several test objects for understanding the performance and limitations of the AM process have been suggested. While these incorporated surface roughness, they do not focus on surface roughness and angular dependency.

Strano et al. [21] and Cabanettes et al. [3] suggested test objects which focused on how the surface roughness depends on the angle, however, both seamed unpractical.[3; 21] The one suggested by Strano et al. [21] did not have internal surfaces and the one suggested by Cabanettes et al. [3] had separate components for each angle. Furthermore, Vandenbroucke and Kruth [27] suggested a test object rather similar to the one by Strano et al. [21], however, with fewer surfaces. [21; 27]

In this thesis, an attempt was done to design a more practical test object which would focus on roughness measurements and angular dependence. For the object to be practical, it should have internal and external surfaces and be able to stand on it self while keeping a surface level. This to make measurements easier.

The three-dimensional polygon was thought to solve several problems. It would allow for internal and external surfaces with discrete angles and it would allow the object to stand on itself while keeping the surfaces level. To find the appropriate number of sides of this polygon, three objects was produced with six, eight and ten sides. From measurements on these it became evident that a twelve-sided object would be proficient. In order to make the object more appropriate for XCT measurements, the height of the twelve-sided test object was decreased by half.

The main components used in this thesis was produced on a `3D Systems Prox DMP 300` using AlSi12, a layer thickness of $30\mu m$ and a beam diameter of approximately $0.1mm$. After printing, all sides where brushed to remove excess dust and loose particles.

The six-sided component was constructed as a hexagon inscribed in a circle with a diameter of 45mm, a height of 25mm and a thickness of 3mm. Each surface had an area of 25mm by 23mm, shown in 1. The eight-sided component was constructed as an octagon inscribed in a circle with a diameter of 43mm, a height of 25mm and a thickness of 3mm. Each surface has an area of 25mm by 17mm, shown in 2. The ten-sided component was constructed as a decagon inscribed in a circle with a diameter of 41mm, a height of 25mm and a thickness of 3mm. Each surface had an area of 25mm by 13mm, shown in 3. The twelve-sided component was constructed as a dodecagon inscribed in a circle with a diameter of 41mm, a height of 13mm and a thickness of 3mm. Each surface had an area of 13mm by 10mm, shown in 4.

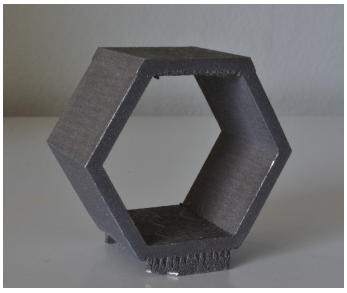

Figure 1: Image of the six sided test object

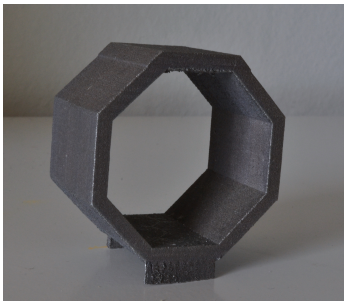

Figure 2: Image of the eight sided test object

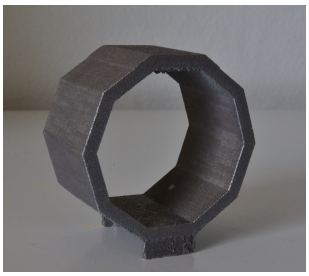

Figure 3: Image of the ten sided test object

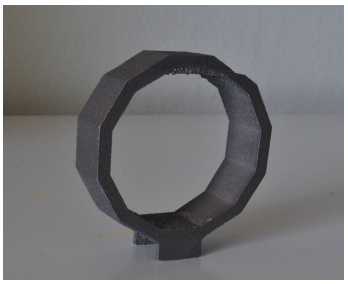

Figure 4: Image of the twelve sided test object

6 Experimental

6.1 Focused variant microscope

The measurements was performed on an `Alicona infinitive focus`, a focus variant microscope, using the surface characterizations setting. 200x magnification (20x lens), polarized light, a vertical resolution of $2\mu m$, lateral resolution of $50nm$, and a cut off frequency of 250 μm was used, as suggested by Cabanettes et al. [3]. In each measurement an imagefield was used and the four most homogenic frames was selected. These represented an area of $0.995mm$ by $1.34mm$. The measurements of the six, eight and ten sided test object was done with an exposure of $181\mu s$, and a of contrast 0.57. However, this produced images which appeared to be a bit too dark and to further improve the measurements of the twelve sided test object exposure and contrast was set to 209 μs and 0.9. In all measurements test object was placed to make the surface as level as possible.

To describe the angle of the surface the following notation was used. Assuming that the vertical side is denoted as 0 degrees, the downward facing sides are -30 and -60 degrees and upwards facing sides are +30, +60 and +90 degrees etc. The six sided object has the angles [-30,30,90] degrees and the eight sided test object [-45,0,45,90] degrees, an example is shown in figure 5.

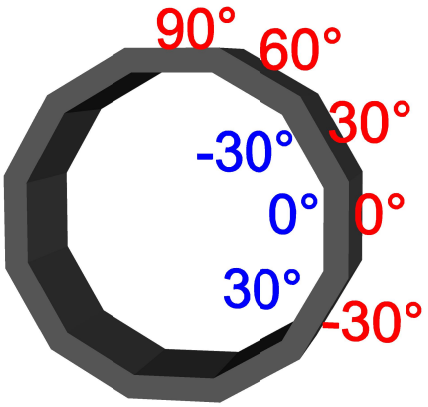

Figure 5: Schematic describing the notation of the surface with corresponding angles. Red numbers are external surfaces, blue are internal surfaces

Initially the data recorded at each angle was fitted with a trigonometrical function. The trigonometrical approach had been suggested by Cabanettes et al. [3] and fitting was done with the RMS method, previously described. The hypothesis was that the surface roughness should repeat it self after 180 degrees, i.e. that the surfaces 270 degrees from printing and 90 degrees from printing should be the same. The equation used in the fit was of the following form:

$$a_0 + a_1 \cos(\alpha w) + b_1 \sin(\alpha w) \tag{15}$$

a_0, a_1, b_1 and w are different constants and α the angle of printing. Using this model and the data recorded from measurements on all five sides of the six sided test object and the seven sides of the eight sided test object, a preliminary model for several parameters was created. For each parameter fitting the data was first controlled such that it was distributed over the entire period and the following parameters was deemed to meet these conditions: S_a, S_q, S_p, S_z, S_{sk}, S_{dq}, and S_{dr}.

From this a prediction of the values of said parameters was done for the ten sided test object and the angles, [-54,-18,18,54,90]. Using the same parameters as for the eight and six sided test object the measurement procedure was redone on all nine sides of the ten sided test

object. From these measurements it is evident that this model did not accurately predict the parameters.

The use of a trigonometric model for the roughness provided estimates which gave a hint of the actual value. However, by simulating the roughness using a third degree polynomial, equation 16,the roughness could be predicted with far better accuracy. This also allows for much more facile modelling of new data. The fitting was done using by using the RMS method and an initial guess of all coefficients was zero.

$$f(\alpha) = a_0 + a_1\alpha + a_2\alpha^2 + a_3\alpha^3 \tag{16}$$

Where a_0, a_1,a_2,a_3 are constants and α is the angle. From the measurements performed on the six,eight and ten sided polygons the conclusion was that using a twelve side test object would yield a sufficient model. The twelve sided test object would give six unique surfaces and by performing repeated measurements on all surfaces it would be possible to establish a model using a single component if all sides was measured three times.

In total 18 data points were collected and a fitting was done using the previously described third degree polynomial, and to that fitting a confidence interval of 95% was done.

Line parameters was measured on the ten-sided test object, using the Alicona line roughness setting. The same cut off frequency of 250 μm as well as contrast 0.9 , exposure 209 μm, and 200x lens was used. Measurements was done both along and across the weld tracks. Images of the surface on the ten sided test object was captured using 25x and 50x times magnification. An attempt to measure the bottom surface was done, however, the extremely rough nature of this surface and the residual support structure deemed it useless.

6.2 X-ray tomography

XCT scans of the 0, + 60 and -60 sides where done to determine whether the external measurements can be transferred to internal measurements. `Zeiss Xradia XRM520` was used to perform all scans with a voxels size of 16μm and an acceleration voltage of 110 kV for 0 and +60 degrees and 80 kV for -60 degrees. The scans resulted in several `.tif` images. These were converted to a greyscale stack using the software `fiji`. Images that upon visual inspection appeared to be part of the surface on either side of the sample was exported. These were then imported into Matlab for further analysis.

Each image was converted to a numerical matrix and the stack of images was summarized to form a single matrix. The matrix describes the topography of the surface very similar to how the FVM generates a surface. In order to further mimic the FVM measurements an area of approximately 1 mm by 1 mm was selected somewhere in the center of each sample.

The S_a was calculated as the absolute of the deviation of the mean integrated, summarized and divided by the area. S_p maximum peak height and S_v maximum pit depth was also calculated using the matlab functions max and min. S_a is as previously described the absolute deviation of the mean by area. To accomplish this the following calculation was done.[9]

$$S_a = \frac{1}{A} \sum \left(\sum \left(|Z(x,y)| \right) dx \right) dx \tag{17}$$

S_q, S_z, S_{sk} and S_{ku} was also calculated using the described equations and the same approximation as for S_a.

7 Results

7.1 Measurement protocol

The protocol which was one of the main objects of this thesis have been determined to the following procedure.

Produce an equilateral twelve sided polygon with a hollow inside and internal surfaces parallel to the external. Remove this from the build plate using a grinder, remove residual support structure and remove any loose particles using a brush or similar.

Perform three repeated measurements on each unique side using a Alicona FVM, 200x magnification (20x lens), 50 nm lateral resolution, 2 μm vertical resolution and an imagefield of 1mm by 1 mm. Use Alicona software or similar to calculate the extended roughness parameters of the measured surfaces. The three values of each parameter at each angle can then be used to determine the variance of said parameter at the given angle.

Roughness parameter values can then be estimated for all other angles by doing a fitting of a third degree polynomial function as displayed in equation 16. Using the initial guess of zero for all coefficients. Repeating the same procedure for the upper and lower bounds of a 95 % confidence interval gives a more accurate representation of what roughness values one can expect. All code and algorithms for the calculations necessary are available on GitHub.

7.2 Roughness measurements - FVM

Images of the surface of the ten sided test object was captured and displayed in figure 6.

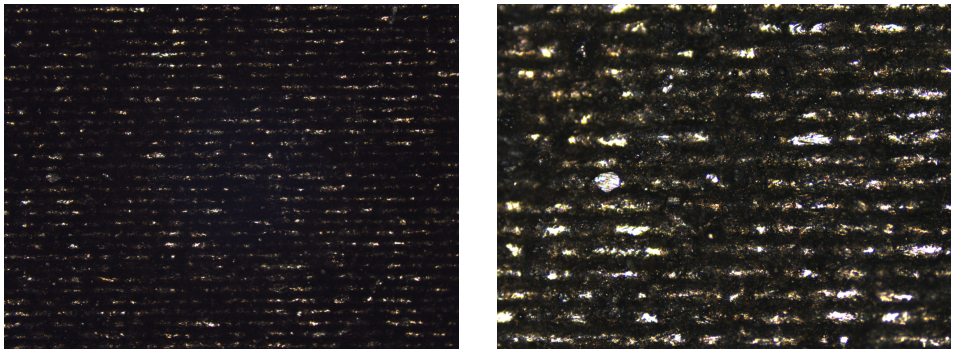

Figure 6: Images of the 90 degree surface on the ten sided test object, left 2.5 times magnification right 5 times magnification

Line parameters was measured on the 90 degree surface of the ten sided test object, the results of this is displayed in table 1.

Table 1: Line parameters measured on the 90 degree surfaces of the ten sided test object

Parameter $[\mu m]$	**Across**	**Along**
R_a	4.799	5.933
R_q	5.663	8.132
R_z	17.930	27.320
R_p	15.086	22.078
R_v	10.361	31.341

The measurements from the FVM of the six sided test object are displayed in table 2 the -30 and 30 degree surface have been measured twice and the 90 degree surface has been measured once. The average of these measurements are displayed in table 2.

Table 2: Average roughness parameters measured with FVM on the six sided test object (Raw data in table 7)

Parameter \ Angle[°]	−30	30	90
Sa [μm]	9.3965	9.0655	5.178
Sq [μm]	11.9005	11.701	7.919
Sp [μm]	53.7165	59.095	76.762
Sv [μm]	46.996	47.9885	49.208
Sz [μm]	100.712	107.0835	125.970
S10z [μm]	98.2435	103.427	124.482
Ssk	0.352	0.2495	1.598
Sku	3.359	3.697	11.369
Sdq	2.627	2.462	1.615
Sdr %	188.605	160.8345	72.449
Exposure [μs]	181	181	181
Contrast	0.57	0.57	0.57

The measurements from the FVM of the eight sided test object are displayed in table 3 where the -45, 0 and 45 degree surface have been measured twice and the 90 degree surface has been measured once. The average of these measurements are displayed in table 3.

Table 3: Average roughness parameters measured with FVM on the eight sided test object (Raw data in table 8)

Parameter \ Angle[°]	−45	0	45	90
Sa [μm]	17.2105	8.3805	12.0905	4.517
Sq [μm]	22.4455	10.551	15.5705	6.271
Sp [μm]	86.5905	38.6605	67.2065	42.556
Sv [μm]	147.7165	50.3105	59.651	32.935
Sz [μm]	234.307	88.971	126.8575	75.491
S10z [μm]	220.4615	87.0475	124.2735	65.985
Ssk	0.0935	−0.5005	0.424	0.603
Sku	3.8545	3.3485	3.6085	5.848
Sdq	4.8145	1.869	3.044	1.046
Sdr %	675.98	101.709	253.0225	34.978
Exposure [μs]	181	181	181	181
Contrast	0.57	0.57	0.57	0.57

The measurements from the FVM of the ten sided test object are displayed in table 4 where the -54,-18, 18, and, 54 degree surface have been measured twice and the 90 degree surface has been measured once. The average of these measurements are displayed in table 4.

Table 4: Average roughness parameters measured with FVM on the ten sided test object (Raw data in table 9)

Parameter \ angle[°]	−54	−18	18	54	90
Sa [μm]	19.241	7.999	8.945	10.1545	5.636
Sq [μm]	25.3535	10.155	11.646	13.313	7.980
Sp [μm]	104.6135	44.258	61.025	60.306	90.369
Sv [μm]	132.8015	47.993	51.84	68.4095	51.678
Sz [μm]	237.4145	92.251	112.865	128.715	142.047
S10z [μm]	235.197	90.393	111.2655	126.4925	140.684
Ssk	−0.149	−0.227	0.2495	0.347	0.663
Sku	3.850	3.317	4.106	3.9805	8.572
Sdq	5.5715	1.991	2.331	2.430	1.453
Sdr %	917.052	114.073	147.134	168.471	64.099
Exposure [μs]	181	181	181	181	181
Contrast	0.57	0.57	0.57	0.57	0.57

The measurements from the FVM of the twelve-sided test object are displayed in table 5. All surfaces have been measured three times and the average of these measurements are displayed in table 4.

Table 5: Average roughness parameters measured with FVM on the twelve sided test object (Raw data in table 10)

Parameter \ angle[°]	−60	−30	0	30	60	90
Sa [μm]	25.0113	12.7590	10.4707	10.4317	11.3773	5.2900
Sq [μm]	32.5627	16.7957	13.3397	13.8897	15.1840	7.6380
Sp [μm]	137.2057	79.9197	68.4213	76.2997	77.0410	64.4387
Sv [μm]	177.7663	67.6033	56.2960	59.8767	58.9010	55.5943
Sz [μm]	314.9723	147.5227	124.7173	136.1763	135.9423	120.0323
S10z [μm]	303.2763	144.2970	122.5000	130.5843	132.0100	95.8013
Ssk	−0.4873	0.4137	0.3067	0.6613	0.7980	1.4510
Sku	4.0683	3.8647	3.6150	4.3923	4.1863	9.4570
Sdq	6.2690	3.9767	3.5367	3.1590	3.4060	1.3510
Sdr %	1150.5607	407.9537	324.6370	267.8340	307.5133	53.6533
Exposure [μs]	209	209	209	209	209	209
Contrast	0.9	0.9	0.9	0.9	0.9	0.9

The digital surface generated by the FVM of the -30, 0,30 and 90 degree surface of the twelve sided test object are displayed in figure 7-10.

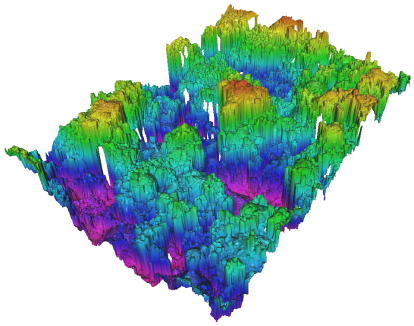

Figure 7: A 3D representation of the -30 degree surface of the twelve sided test object

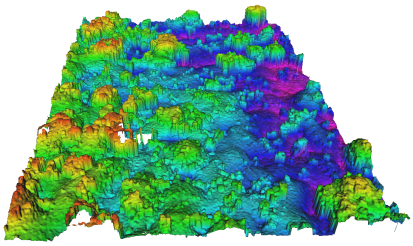

Figure 8: A 3D representation of the 0 degree surface of the twelve sided test object

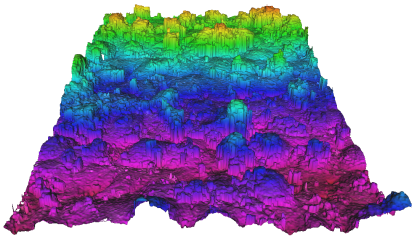

Figure 9: A 3D representation of the 30 degree surface of the twelve sided test object

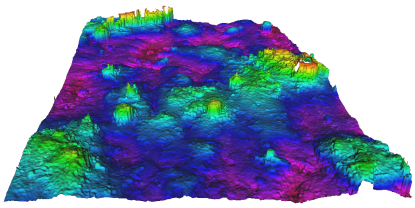

Figure 10: A 3D representation of the 90 degree surface of the twelve sided test object

7.3 Simulation of Roughness parameters

The data found in table 5 was fitted using the previously described RMS method and the result of this and a fitting to the confidence interval is shown in the following figures.

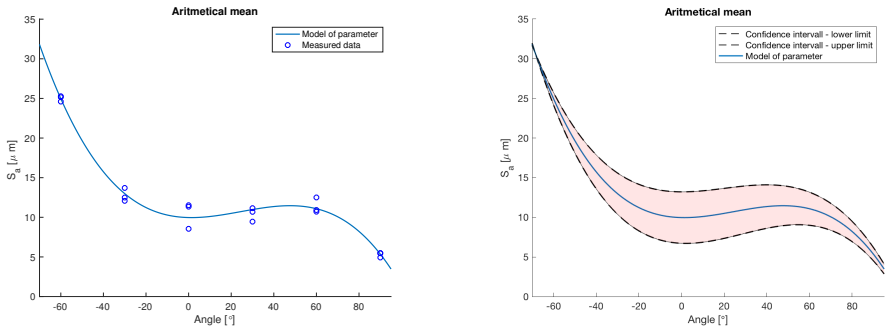

Figure 11: Left S_a data of the twelve sided test object with fitted polynomial, right fitted polynomial with 95% confidence interval marked as the red area.

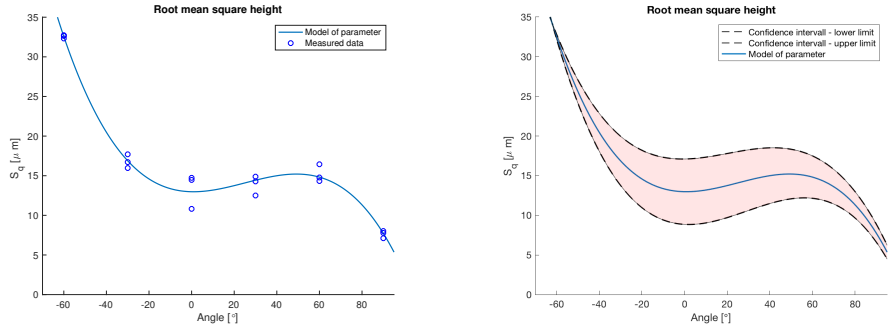

Figure 12: Left S_q data of the twelve sided test object with fitted polynomial, right fitted polynomial with 95% confidence interval marked as the red area.

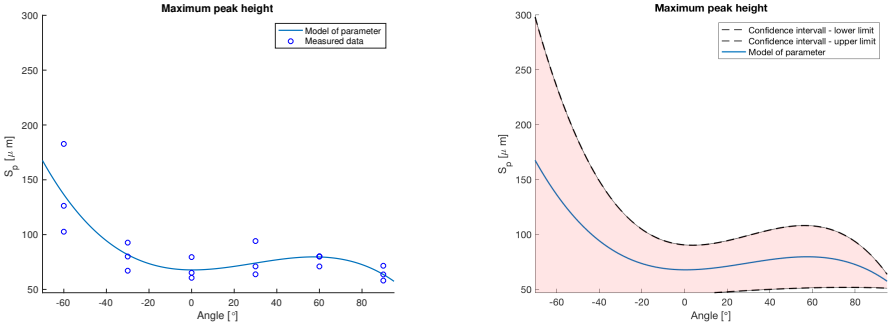

Figure 13: Left S_p data of the twelve sided test object with fitted polynomial, right fitted polynomial with 95% confidence interval marked as the red area.

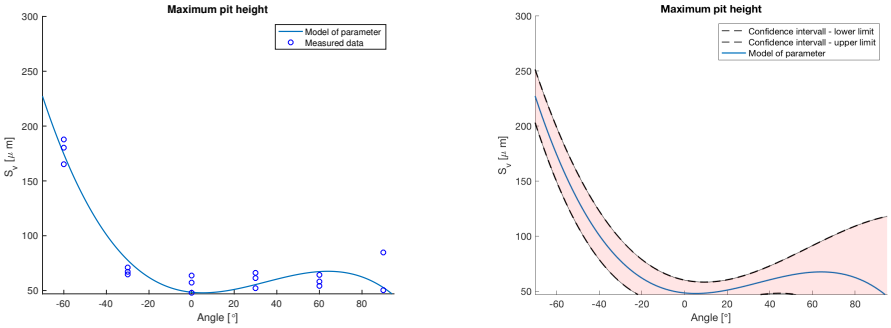

Figure 14: Left S_v data of the twelve sided test object with fitted polynomial, right fitted polynomial with 95% confidence interval marked as the red area.

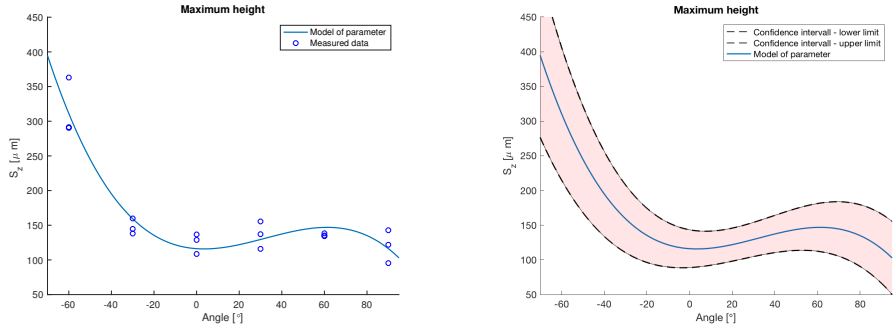

Figure 15: Left S_z data of the twelve sided test object with fitted polynomial, right fitted polynomial with 95% confidence interval marked as the red area.

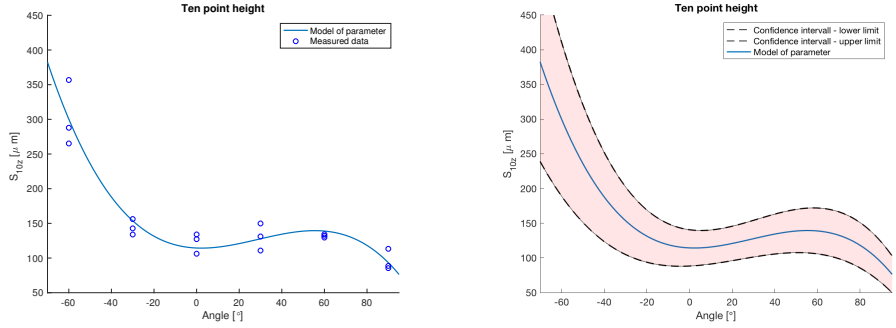

Figure 16: Left S_{10z} data of the twelve sided test object with fitted polynomial, right fitted polynomial with 95% confidence interval marked as the red area.

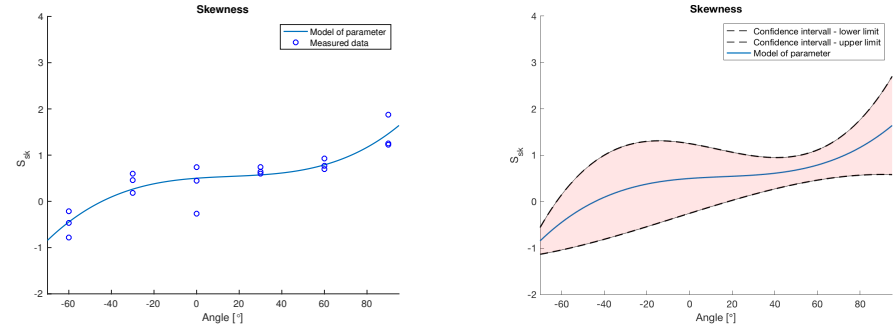

Figure 17: Left S_{sk} data of the twelve sided test object with fitted polynomial, right fitted polynomial with 95% confidence interval marked as the red area.

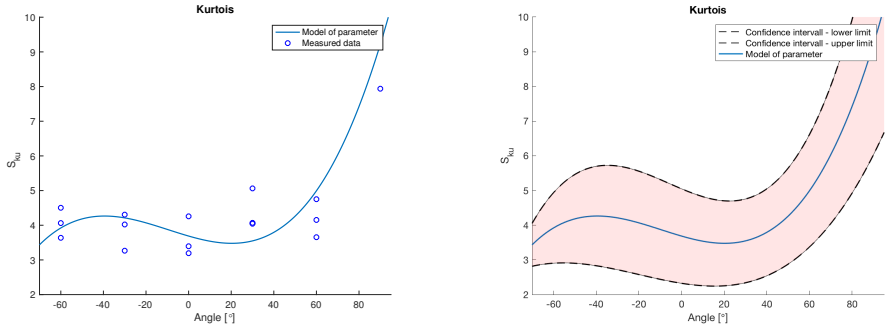

Figure 18: Left S_{ku} data of the twelve sided test object with fitted polynomial, right fitted polynomial with 95% confidence interval marked as the red area.

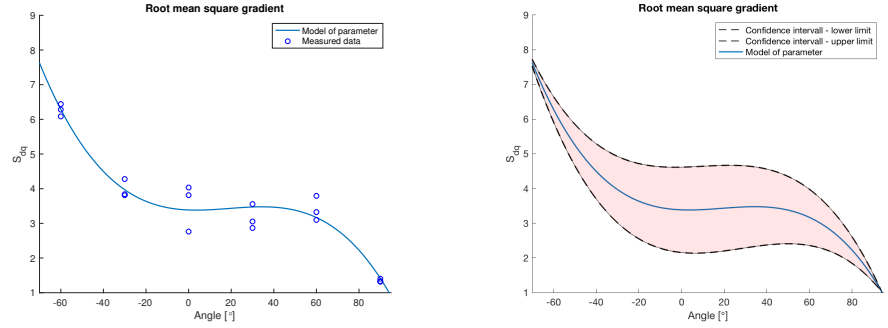

Figure 19: Left S_{dq} data of the twelve sided test object with fitted polynomial, right fitted polynomial with 95% confidence interval marked as the red area.

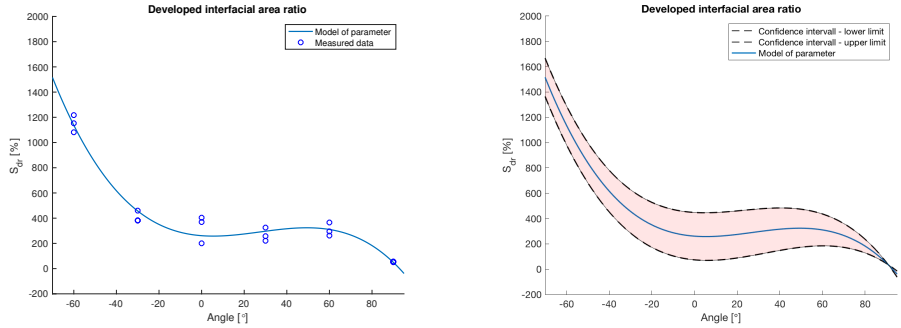

Figure 20: Left S_{dr} data of the twelve sided test object with fitted polynomial, right fitted polynomial with 95% confidence interval marked as the red area.

7.4 X-ray generated surfaces

The images from the XCT performed on the twelve sided test object was generated as previously described and the results of this is displayed in the following figures.

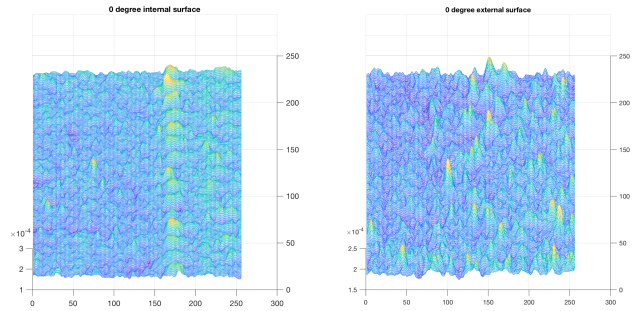

Figure 21: The internal and external surfaces generated from the 0 degree surface in the twelve sided test object

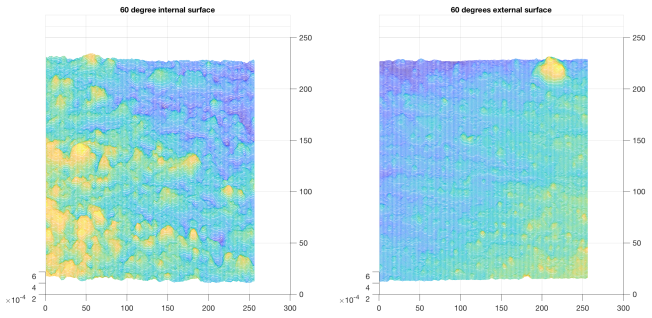

Figure 22: The internal(-60 degrees) and external(60 degrees) surfaces generated from the 60 degree surface in the twelve sided test object

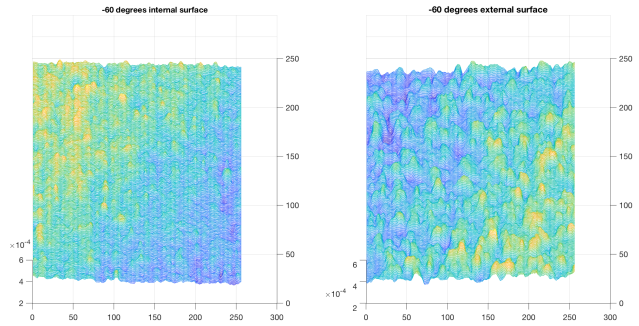

Figure 23: The internal (60 degrees) and external(-60 degrees) surfaces generated from the -60 degree surface in the twelve sided test object

From the generated the surfaces roughness parameters was calculated and these are displayed in the following table.

Table 6: Roughness parameters calculated for three angles as of the data recorded from XCT

Surface / Parameter	0 degrees		60 degrees		-60degrees	
	Internal	External	Internal	External	Internal	External
S_a [μm]	5.403	5.621	25.285	12.566	14.133	21.210
S_q [μm]	7.182	7.644	31.259	16,623	17.183	26.493
S_p [μm]	49.626	52.301	112.18	74.906	67.406	112.41
S_v [μm]	32.702	23.108	113.18	74.271	55.882	83.634
S_z [μm]	82.327	75.408	225.35	149.17	123.29	196.04
S_{sk}	2.1285	1.9462	1.7985	1.5387	1.5011	1.5830
S_{ku}	5.2157	6.4319	2.7442	3.9470	2.6190	2.9537

8 Discussion

8.1 FVM

On the 90-degree surface as seen in figure 6, the weld tracks are clearly distinguishable lines. These are present on all of the surface, however, most evident on the 90-degree surface.

Comparing the line parameters displayed in table 1 with the extended parameters this shows that S_a, R_a, S_q and R_q share a high degree of similarity. The R_a measured across the weld tracks and along the weld track, although different they are both similar to the S_a and S_q. Line parameters are more sensitive than the extended parameters, however, these differences could be due to random irregularities.[15] The other line parameters differ more from the extended parameters R_p, R_v, and R_z. This is expected since these are extreme value parameters. The large difference from the extended parameter can be explained since the chance of including a high or low peak is greater on a surface than on a line.

The notation suggested here is different to the notation most commonly used. However, it gives the possibility to replaces the use of down-skin and up-skin surfaces with positive and negative angles. The notation also makes modeling much more facile since negative and positive can be described mathematically. When discussing the results and making more general assumptions the use of horizontal (90 degrees) and vertical (0 degrees) surfaces become more useful as well as upskin (positive angles) and downskin (negative values).

From the FVM measurements, we can see that we in general have a higher surface roughness on the down-skin surface and a lower on the up-skin surface. This is very much in line with the previous work done by Cabanettes et al. [3]who found similar behavior. We found that the surface roughness increases with an increasing negative angle and decreases with increasing positive angle.

However, this behavior would give a more or less linear decrease which is not the behavior found, there is a local minimum at the vertical surface. This is then followed by a slight increase before decreasing towards the horizontal surface and the horizontal surface appears to be the least rough of all the surfaces. This trend is evident for S_a (Figure 11), S_q(Figure 12), S_z(Figure 15), and S_{10z}(Figure 16). For S_p(Figure 13) and S_v (Figure 14) a similar trend is present, however, the vertical surface and the horizontal surface are more similar than they are for S_a , S_q S_z and S_{10z}.

The S_{sk} (Figure 17) has an almost linear increase. For the most downskin surface it is less than zero and for the upskin and vertical surface, the value is larger than zero. This gives that for lower angles the height distribution is shifted above the mean plane i.e. more peaks than pits.

S_{ku} (Figure 18) has a typical third-degree polynomial appearance, with a local minimum at around 20 degrees. However, the value is always larger than 3 which indicates that the surfaces have an increasing tendency to form a narrow height distribution, higher peaks and more consistent peak heights.

Both S_{dq} (Figure 19) and S_{dr} (Figure 20) follow the same type of behavior as S_a,S_q, S_z, and S_{10z}. The S_{dq} indicates that the slope of the surface decreases with increasing angle which could be due to the slight distortion of the test object.

The interfacial area ratio, S_{dr}, behaves similarly to S_a. This indicates that the increase in surface area is larger for the vertical surface than the horizontal. A very low S_{dr} is evident for the horizontal surface, only 53% compared to the value for the -60 degree surface which is more than 1000%. This can be of interest for a few applications such as heat transfer, where a large surface area is of value and hence a large S_{dr} could be favorable. [24] From the values of S_a, S_p, S_v and S_z we can show that the peaks are generally higher than the pits, however, at horizontal and vertical surfaces the pit and peaks are almost the same height. The exception is the -60-degree surface in which the peaks are lower than the pits. This is also confirmed by the S_{sk} which is negative for -60 and positive for all other surfaces.

S_a, S_q, S_{dq}, and S_{dr} have a higher variance for the vertical surface and lower for both negative and horizontal surfaces. In contrast, the variance for S_v, S_p, S_z, S_{z10},S_{sk}, and S_{ku} have a more constant variance. The lower variance would indicate that we have a more homogeneous surface at the lowest and highest angles, and more shifting surfaces close to the vertical surface.

Generally we can say that most parameters have their lowest value around horizontal external surfaces or vertical surfaces, however, it should be noted that close to horizontal external surface have a very spiked height distribution i.e. a high S_{ku}.

Cabanettes et al. [3] suggested a larger image field than what was chosen to be used in this project. This was mostly due to the equipment used in this project, as the time for measurements of this size was too long. However, the use of multiple measurements did not only decrease the time of measuring but also gave a possibility to calculate and understand the variance of the parameters.

The image field used by Cabanettes et al. [3] was four times large than the one used, and to be more consistent with their work repeating these measurements four times instead of three could have been interesting. However, the use of only three measurements have proved to give sufficient data both for the confidence interval calculations as well as the polynomial fittings. On some of the surfaces a slight angle can be noted, this could be be compensated for in the software. This was not done in order to keep the procedure as simple as possible. However, a slope should not affect the roughness in any significant manner since the slope is present across the whole surface which is also confirmed by the seemingly normal S_{dq}

8.2 XCT

For all surface, a corresponding internal surface exists and has the same angle as the external since they are parallel. However, for the horizontal surface this surface is not measurable due to the presence of support structure, which is necessary for the component to be fabricated. Unless noted the expressions horizontal and vertical surfaces refers to the external surfaces. To investigate the relations between internal surface and external surfaces the XCT measurements was performed.

The results of the XCT measurements and the calculations of the roughness parameters are in line with the measurements done by the FVM. Although not that facile or straightforward as the FVM this method provided very interesting results and gave insight in more than just the surface. It was evident that throughout the sample, the weld tracks which are clearly

distinguishable on the surface, as seen in figure 6.However, these are not present in the internal structure which in turn shows that a complete weld has been formed and no internal macrostructures could be observed.

Furthermore, the roughness parameters calculated from the XCT measurements (table 6) indicates that the two surfaces from the 0-degree portion are very similar and the difference could be within an error margin. These surfaces also share a visual similarity as seen in figure 21. Measurements of the component which originates from the -60 and 60-degree surfaces show that in both cases the external surface differs from the internal surface.

The initial hypothesis was that the external surface of -60 would be the same as the internal surface on 60 hence making it possible to measure an external surface to understand an internal surface. In the measurements of these external surfaces (-60 degrees,60 degrees) several parameters show a higher degree of similarity with their internal counterpart.

The appearance of these surfaces as shown in figure 22 and figure 23 also indicates that the internal surfaces and external surfaces could be interchangeable. However, given the large variance which we have seen in the FVM measurements, the evidence is not strong enough to clearly say that these surfaces are interchangeable. It is my belief that upon further investigation this will be confirmed.

8.3 Improvements and future work

The earliest measurements were performed on unbrushed components which makes these results less reliable. Furthermore, the use of the FVM has a certain degree of skill to it, so the later measurements should be more reliable. During the fabrication process of the twelve-sided component, the coater got caught on the component which caused a slight distortion of one side of the component. This distortion did only affect one of the sides and the other was left undisturbed. However, it might have led to that the surfaces was not perfectly leveled when measured.

Although no post-treatment apart from light brushing was done on the components and that this protocol has been developed using only untreated AlSi12 AM components it can hopefully be applied to any material. It should also be applicable for use with sand blasting, shot penning or any other post treatment as well. The protocol might even be applicable to other AM techniques than SLM as well.

The use of contrast and brightness is also needed to be kept constant, this since FVM is more or less an image interpretation technique. However, using a similar protocol it could be possible to investigate how this affects surface roughness. Furthermore, investigating whether the roughness is affected by the area of the surface could be useful. Especially when the area of the surface is approximately the size of the beam, since one interesting application of AM is complex miniature structures.[7]

The final design of the test object showed great promise and fully filled the initial requirements. However, the design could be improved by further decreasing the height of the object and reducing the thickness, to facilitate the XCT measurements and make them faster.

To even further improve the test object, it could be designed to be separable into two halves,

this to make it possible to confirm the internal measurements using conventional techniques. This have previously been done by Thompson et al. [23], in designing a test object for XCT.

8.4 Notation of Roughness

In this work the need for a new notation to describe which surface the given roughness value originates from have become evident. The behavior found in this thesis shows that the parameter value is related to the angle and the placement of the surfaces i.e. external or internal. To highlight this the extended roughness parameters could be used in a subsequent manner. The angle of the surface, in relation to the vertical plane which is perpendicular to the coater, is noted as a number and the letter **i** and **e** is used to describe whether it is measured as an internal surface or an external surface.

The use of **e** could be neglected if the most common surfaces described are external and **i** only used to note that the surface in question is internal. An example of how this could look S^e_{a30} or in a general sense where α is the angle, c the position of the surface and x the notation for the given surface parameter (a,q,p,v,z,sk,...,etc) $S^c_{x\alpha}$. This would allow for a more true and a more understandable way to describe and understand the surface roughness of AM produced components.

Using this type of notation would make it possible for both the academic community and the industry to describe and discuss surface roughness more accurately. To exemplify, a surface with a S_a of 18 μm could be great if the angle is -55 degrees but rather poor if the angle is 0 degrees, hence this notation is needed.

9 Conclusion

In conclusion, we have found that the surface roughness of components produced by additive manufacturing have a significant angular dependency. It has been shown that the measurement protocol which is suggested here can be used to predict and understand the roughness parameters measured. The twelve-sided test object gave sufficient data points while allowing for a relatively fast process. A full set of measurements could be done in an afternoon. Although not confirmed there is evidence in favor of that the external surface roughness can be used to understand the internal surface roughness. The use of a new notation for surface roughness of AM production have been proven necessary and we suggest that the form of $S^p_{x\alpha}$ is the simplest and most useful.

To further improve on this work, the relation of the internal and external surfaces needs to be studied more. If it is possible to prove that an external surface is identical to its corresponding internal surface the positioning notation could be deemed unnecessary. Furthermore, studying if these relationships are true regardless of the area, material or production technique could be of great interest.

10 References

References

[1] A brief history of additive manufacturing and the 2009 roadmap for additive manufacturing: Looking back and looking ahead | request pdf. 2018/8/13/.

[2] E. Atzeni and A. Salmi. Economics of additive manufacturing for end-usable metal parts. *The International Journal of Advanced Manufacturing Technology*, 62(9):1147–1155, Oct 2012. ISSN 1433-3015. doi: 10.1007/s00170-011-3878-1. URL https://doi.org/10.1007/s00170-011-3878-1.

[3] F. Cabanettes, A. Joubert, G. Chardon, V. Dumas, J. Rech, C. Grosjean, and Z. Dimkovski. Topography of as built surfaces generated in metal additive manufacturing: A multi scale analysis from form to roughness. *Precision Engineering*, 52:249 – 265, 2018. ISSN 0141-6359. doi: https://doi.org/10.1016/j.precisioneng.2018.01.002. URL http://www.sciencedirect.com/science/article/pii/S014163591730627X.

[4] A. Cohen, R. Chen, U. Frodis, M. Wu, and C. Folk. Microscale metal additive manufacturing of multi□component medical devices. *Rapid Prototyping Journal*, 16(3):209–215, 2010. doi: 10.1108/13552541011034889. URL https://doi.org/10.1108/13552541011034889.

[5] A. N. Dickson, J. N. Barry, K. A. McDonnell, and D. P. Dowling. Fabrication of continuous carbon, glass and kevlar fibre reinforced polymer composites using additive manufacturing. *Additive Manufacturing*, 16:146 – 152, 2017. ISSN 2214-8604. doi: https://doi.org/10.1016/j.addma.2017.06.004. URL http://www.sciencedirect.com/science/article/pii/S2214860416301889.

[6] W. Erna. Edwards, allen, l.: An introduction to linear regression and correlation. (a series of books in psychology.) w. h. freeman and comp., san francisco 1976. 213 s., tafelanh., s 7.00. *Biometrical Journal*, 19(1):83–84. doi: 10.1002/bimj.4710190121. URL https://onlinelibrary.wiley.com/doi/abs/10.1002/bimj.4710190121.

[7] W. E. Frazier. Metal additive manufacturing: A review. *Journal of Materials Engineering and Performance*, 23(6):1917–1928, Jun 2014. ISSN 1544-1024. doi: 10.1007/s11665-014-0958-z. URL https://doi.org/10.1007/s11665-014-0958-z.

[8] E. Gadelmawla, M. Koura, T. Maksoud, I. Elewa, and H. Soliman. Roughness parameters. 123:133–145, 04 2002.

[9] K. Greet, P. Grzegorz, M. Maarten, V. B. Simon, S. Jan, and W. Martine. High-resolution microfocus x-ray computed tomography for 3d surface roughness measurements of additive manufactured porous materials. *Advanced Engineering Materials*, 15(3):153–158. doi: 10.1002/adem.201200156. URL https://onlinelibrary.wiley.com/doi/abs/10.1002/adem.201200156.

[10] D. Herzog, V. Seyda, E. Wycisk, and C. Emmelmann. Additive manufacturing of metals. *Acta Materialia*, 117:371 – 392, 2016. ISSN 1359-6454. doi: https://doi.org/

10.1016/j.actamat.2016.07.019. URL http://www.sciencedirect.com/science/article/pii/S1359645416305158.

[11] W. Kapłonek, K. Nadolny, and G. M. Królczyk. The use of focus-variation microscopy for the assessment of active surfaces of a new generation of coated abrasive tools. *Measurement Science Review*, 16(2):42 – 53, 2016. URL https://content.sciendo.com/view/journals/msr/16/2/article-p42.xml.

[12] S. A. Khairallah, A. T. Anderson, A. Rubenchik, and W. E. King. Laser powder-bed fusion additive manufacturing: Physics of complex melt flow and formation mechanisms of pores, spatter, and denudation zones. *Acta Materialia*, 108:36 – 45, 2016. ISSN 1359-6454. doi: https://doi.org/10.1016/j.actamat.2016.02.014. URL http://www.sciencedirect.com/science/article/pii/S135964541630088X.

[13] J. Kinney, Q. Johnson, U. Bonse, M. Nichols, R. Saroyan, R. Nusshardt, R. Pahl, and J. M. Brase. Three dimensional x-ray computed tomography in materials science. *MRS Bulletin*, 13(1):13–18, 1988. doi: 10.1557/S0883769400066525.

[14] M. Koike, K. Chan, R. MASON, S. HUMMEL, Y. KOBAYASHI, and T. OKABE. Fatigue life of titanium alloys fabricated by additive-layer manufacturing techniques. 03 2013.

[15] R. Leach. *Characterisation of areal surface texture*. 06 2013.

[16] S. P. Moylan, J. A. Slotwinski, A. Cooke, K. K. Jurrens, and M. Z. Alkan. Proposal for a standardized test artifact for additive manufacturing machines and processes. 2012.

[17] L. E. Murr, S. M. Gaytan, D. A. Ramirez, E. Martinez, J. Hernandez, K. N. Amato, P. W. Shindo, F. R. Medina, and R. B. Wicker. Metal fabrication by additive manufacturing using laser and electron beam melting technologies. *Journal of Materials Science & Technology*, 28(1):1 – 14, 2012. ISSN 1005-0302. doi: https://doi.org/10.1016/S1005-0302(12)60016-4. URL http://www.sciencedirect.com/science/article/pii/S1005030212600164.

[18] L. Pagani, Q. Qi, X. Jiang, and P. J. Scott. Towards a new definition of areal surface texture parameters on freeform surface. *Measurement*, 109:281 – 291, 2017. ISSN 0263-2241. doi: https://doi.org/10.1016/j.measurement.2017.05.028. URL http://www.sciencedirect.com/science/article/pii/S0263224117303068.

[19] S. M. Seitz and C. R. Dyer. Photorealistic scene reconstruction by voxel coloring. *International Journal of Computer Vision*, 35(2):151–173, Nov 1999. ISSN 1573-1405. doi: 10.1023/A:1008176507526. URL https://doi.org/10.1023/A:1008176507526.

[20] C. Shuai, L. Xue, C. Gao, Y. Yang, S. Peng, and Y. Zhang. Selective laser melting of zn–ag alloys for bone repair: microstructure, mechanical properties and degradation behaviour. *Virtual and Physical Prototyping*, 13(3):146–154, 2018. doi: 10.1080/17452759.2018.1458991. URL https://doi.org/10.1080/17452759.2018.1458991.

[21] G. Strano, L. Hao, R. M. Everson, and K. E. Evans. Surface roughness analysis, modelling and prediction in selective laser melting. *Journal of Materials Processing Technology*, 213(4):589 – 597, 2013. ISSN 0924-0136. doi: https://doi.org/10.1016/j.jmatprotec.2012.11.011. URL http://www.sciencedirect.com/science/article/pii/S0924013612003366.

[22] D. Taylor and O. M. Clancy. The fatigue performance of machined surfaces. *Fatigue & Fracture of Engineering Materials & Structures*, 14(2□3):329–336. doi: 10.1111/j.1460-2695.1991.tb00662.x. URL https://onlinelibrary.wiley.com/doi/abs/10.1111/j.1460-2695.1991.tb00662.x.

[23] A. Thompson, L. Körner, N. Senin, S. Lawes, I. Maskery, and R. K. Leach. Measurement of internal surfaces of additively manufactured parts by x-ray computed tomography. February 2017. URL http://eprints.nottingham.ac.uk/48649/.

[24] S. M. Thompson, Z. S. Aspin, N. Shamsaei, A. Elwany, and L. Bian. Additive manufacturing of heat exchangers: A case study on a multi-layered ti–6al–4v oscillating heat pipe. *Additive Manufacturing*, 8:163 – 174, 2015. ISSN 2214-8604. doi: https://doi.org/10.1016/j.addma.2015.09.003. URL http://www.sciencedirect.com/science/article/pii/S2214860415000469.

[25] B. Turner and S. Gold. A review of melt extrusion additive manufacturing processes: Ii. materials, dimensional accuracy, and surface roughness. 21:250–261, 04 2015.

[26] A. Uriondo, M. Esperon-Miguez, and S. Perinpanayagam. The present and future of additive manufacturing in the aerospace sector: A review of important aspects. *Proceedings of the Institution of Mechanical Engineers, Part G: Journal of Aerospace Engineering*, 229(11):2132–2147, 2015. doi: 10.1177/0954410014568797. URL https://doi.org/10.1177/0954410014568797.

[27] B. Vandenbroucke and J. Kruth. Selective laser melting of biocompatible metals for rapid manufacturing of medical parts. *Rapid Prototyping Journal*, 13(4):196–203, 2007. doi: 10.1108/13552540710776142. URL https://doi.org/10.1108/13552540710776142.

[28] R. Walter and M. B. Kannan. Influence of surface roughness on the corrosion behaviour of magnesium alloy. *Materials & Design*, 32(4):2350 – 2354, 2011. ISSN 0261-3069. doi: https://doi.org/10.1016/j.matdes.2010.12.016. URL http://www.sciencedirect.com/science/article/pii/S0261306910007442.

[29] J. Wilkes, Y. Hagedorn, W. Meiners, and K. Wissenbach. Additive manufacturing of zro2□al2o3 ceramic components by selective laser melting. *Rapid Prototyping Journal*, 19(1):51–57, 2013. doi: 10.1108/13552541311292736. URL https://doi.org/10.1108/13552541311292736.

[30] K. Wong, A. H.-I. M. Engineering, and 2012. A review of additive manufacturing. 2012. URL http://downloads.hindawi.com/journals/isrn.mechanical.engineering/2012/208760.pdf.

[31] E. Wycisk, A. Solbach, S. Siddique, D. Herzog, F. Walther, and C. Emmelmann. Effects of defects in laser additive manufactured ti-6al-4v on fatigue properties. *Physics Procedia*, 56:371 – 378, 2014. ISSN 1875-3892. doi: https://doi.org/10.1016/j.phpro.2014.08.120. URL http://www.sciencedirect.com/science/article/pii/S187538921400265X. 8th International Conference on Laser Assisted Net Shape Engineering LANE 2014.

11 Appendix

Table 7: FVM data of the six-sided test object

Parameter \ Angel[°]	-90	-30	30	90	30	-30
Sa	23,755	8,392	9,189	5,178	8,942	10,401
Sq	32,133	10,749	11,932	7,919	11,47	13,052
Sp	168,663	46,742	55,351	76,762	62,839	60,691
Sv	190,882	45,910	44,758	49,208	51,219	48,082
Sz	359,545	92,651	100,109	125,970	114,058	108,773
S10z	308,351	90,096	98,917	124,482	107,937	106,391
Ssk	0,156	0,219	0,357	1,598	0,142	0,485
Sku	4,809	3,374	3,862	11,369	3,532	3,344
Sdq	8,484	2,394	2,465	1,615	2,459	2,860
Sdr %	1780,814	148,705	169,799	72,449	151,870	228,505
FlTr	359,545	92,651	100,109	125,970	114,058	108,773
Lc	250	250	250	250	250	

Table 8: FVM data of the eight-sided test object

Parameter \ Angel[°]	-45	0	45	90	45	90	-45
Sa [um]	11,628	8,530	11,014	4,517	13,167	8,231	22,793
Sq [um]	15,501	10,647	14,168	6,271	16,973	10,455	29,390
Sp [um]	66,242	39,907	57,845	42,556	76,568	37,414	106,939
Sv [um]	64,507	46,652	57,269	32,935	62,033	53,969	230,926
Sz [um]	130,749	86,559	115,114	75,491	138,601	91,383	337,865
S10z [um]	123,849	85,895	112,431	65,985	136,116	88,20	317,074
Ssk	0,526	−0,233	0,219	0,603	0,629	−0,768	−0,339
Sku	3,824	3,063	3,457	5,848	3,760	3,634	3,885
Sdq	3,409	1,912	2,813	1,046	3,275	1,826	6,220
Sdr %	314,182	104,326	212,990	34,978	293,055	99,092	1037,778
FlTr	130,749	86,559	115,114	75,491	138,601	91,383	337,865
Lc [um]	250	250	250	250	250	250	250
Exposure	181	181	181	181	181	181	181
Contrast	0,57	0,57	0,57	0,57	0,57	0,57	0,57
Vertical resolution [nm]	2	2	2	2	2	2	2
Lateral resolution [um]	50	50	50	50	50	50	50

Table 9: FVM data of the ten-sided test object

Parameter \ Angel[°]	-54	-18	18	54	90	54	18	-18	-54
Sa [um]	13,212	7,991	8,254	11,083	5,636	9,226	9,636	8,007	25,27
Sq [um]	17,088	10,042	11,089	14,544	7,980	12,082	12,203	10,268	33,619
Sp [um]	73,171	45,810	59,808	68,182	90,369	52,430	62,242	42,706	136,056
Sv [um]	77,201	45,868	56,418	85,149	51,678	51,670	47,262	50,118	188,402
Sz [um]	150,371	91,678	116,226	153,331	142,047	104,099	109,504	92,824	324,458
S10z [um]	148,295	87,962	113,135	151,777	140,684	101,208	109,396	92,824	322,099
Ssk	0,053	−0,257	0,558	0,396	0,663	0,298	−0,059	−0,197	−0,351
Sku	3,453	3,127	4,940	3,991	8,572	3,970	3,272	3,507	4,247
Sdq	3,911	1,825	2,410	2,589	1,453	2,271	2,252	2,157	7,232
Sdr %	407,133	100,477	148,969	191,141	64,099	145,801	145,299	127,669	1426,971
FlTr	150,371	91,678	116,226	153,331	142,047	104,099	109,504	92,824	324,458
Lc [um]	250	250	250	250	250	250	250	250	250
Exposure	181	181	181	181	181	181	181	181	181
Contrast	0,57	0,57	0,57	0,57	0,57	0,57	0,57	0,57	0,57
Vertical resolution [nm]	50	50	50	50	50	50	50	50	50
Lateral resolution [um]	2	2	2	2	2	2	2	2	2

30	**30**	**30**	**60**	**60**	**60**	**90**	**90**	**90**
9,453	11,153	10,689	10,918	10,710	12,504	4,928	5,468	5,474
12,504	14,884	14,281	14,778	14,330	16,444	7,112	7,781	8,021
63,790	70,987	94,122	79,974	70,958	80,191	71,580	58,076	63,660
52,140	66,125	61,365	54,223	64,276	58,204	50,314	84,738	31,731
115,930	137,111	155,488	134,197	135,234	138,396	121,894	142,813	95,390
110,798	131,104	149,851	129,528	132,120	134,382	113,315	88,644	85,445
0,642	0,6	0,742	0,927	0,770	0,697	1,253	1,225	1,875
4,044	4,070	5,063	4,751	4,153	3,655	10,194	7,938	10,239
2,867	3,556	3,054	3,325	3,100	3,793	1,317	1,404	1,332
220,816	325,409	257,277	294,937	261,864	365,739	50,469	55,537	54,954
115,930	137,111	155,488	134,197	135,234	138,396	121,894	142,813	95,390
250	250	250	250	250	250	250	250	250
209	209	209	209	209	209	209	209	209
0,9	0,9	0,9	0,9	0,9	0,9	0,9	0,9	0,9
50	50	50	50	50	50	50	50	50
2	2	2	2	2	2	2	2	2

Table 10: FVM data of the twelve-sided test object

Angel[°] / Parameter	-60	-60	-60	-30	-30	-30	0	0	0
Sa [um]	25,275	25,156	24,603	12,494	12,078	13,705	11,524	11,340	8,548
Sq [um]	32,640	32,730	32,318	16,717	15,969	17,701	14,734	14,468	10,817
Sp [um]	126,273	102,636	182,708	92,684	80,011	67,064	79,486	65,185	60,593
Sv [um]	165,199	187,792	180,308	67,121	64,690	70,999	57,233	63,671	47,984
Sz [um]	291,473	290,428	363,016	159,804	144,701	138,063	136,719	128,856	108,577
S10z [um]	287,855	265,227	356,747	156,221	142,766	133,904	134,021	127,249	106,230
Ssk	−0,466	−0,782	−0,214	0,599	0,459	0,183	0,740	0,446	−0,266
Sku	3,638	4,063	4,504	4,306	4,022	3,266	4,257	3,394	3,194
Sdq	6,281	6,441	6,085	3,812	3,840	4,278	4,033	3,814	2,763
Sdr %	1152,840	1217,468	1081,374	381,715	382,197	459,949	403,986	369,326	200,599
FlTr	291,473	290,428	363,016	159,804	144,701	139,063	136,719	128,856	108,577
Lc [um]	250	250	250	250	250	250	250	250	250
Exposure	209	209	209	209	209	209	209	209	209
Contrast	0,9	0,9	0,9	0,9	0,9	0,9	0,9	0,9	0,9
Vertical resolution [nm]	50	50	50	50	50	50	50	50	50
Lateral resolution [um]	2	2	2	2	2	2	2	2	2